NANO · MICRO small
www.small-journal.com

Self-Healing, Adhesive, and Highly Stretchable Ionogel as a Strain Sensor for Extremely Large Deformation

Li Mei Zhang, Yuan He, Sibo Cheng, Hao Sheng, Keren Dai, Wen Jiang Zheng, Mei Xiang Wang, Zhen Shan Chen, Yong Mei Chen, and Zhigang Suo*

Fabricating a strain sensor that can detect large deformation over a curved object with a high sensitivity is crucial in wearable electronics, human/machine interfaces, and soft robotics. Herein, an ionogel nanocomposite is presented for this purpose. Tuning the composition of the ionogel nanocomposites allows the attainment of the best features, such as excellent self-healing (>95% healing efficiency), strong adhesion (347.3 N m^{-1}), high stretchability (2000%), and more than ten times change in resistance under stretching. Furthermore, the ionogel nanocomposite–based sensor exhibits good reliability and excellent durability after 500 cycles, as well as a large gauge factor of 20 when it is stretched under a strain of 800–1400%. Moreover, the nanocomposite can self-heal under arduous conditions, such as a temperature as low as –20 °C and a temperature as high as 60 °C. All these merits are achieved mainly due to the integration of dynamic metal coordination bonds inside a loosely cross-linked network of ionogel nanocomposite doped with Fe_3O_4 nanoparticles.

L. M. Zhang, Y. He, S. Cheng, H. Sheng, Z. S. Chen, Prof. Y. M. Chen
State Key Laboratory for Strength and Vibration of Mechanical Structures
School of Aerospace
Xi'an Jiaotong University
Xi'an 710049, China
E-mail: chenym@mail.xjtu.edu.cn

Dr. K. Dai
ZNDY of Ministerial Key Laboratory
School of Mechanical Engineering
Nanjing University of Science and Technology
Nanjing 210094, China

Dr. W. J. Zheng, Dr. M. X. Wang
State Key Laboratory for Mechanical Behaviour of Materials of Physics
School of Science
Xi'an Jiaotong University
Xi'an 710049, China

Prof. Y. M. Chen
College of Bioresources Chemical and Materials Engineering
National Demonstration Center for Experimental Light Chemistry Engineering Education
Shaanxi University of Science & Technology
Xi'an 710021, China

Prof. Z. Suo
Kavli Institute for Bionano Science and Technology
John A. Paulson School of Engineering and Applied Science
Harvard University
Cambridge, MA 02138, USA

The ORCID identification number(s) for the author(s) of this article can be found under https://doi.org/10.1002/smll.201804651.

DOI: 10.1002/smll.201804651

Self-healing, stretchability, sensitivity, and conformability are vital features of muscles. The development of soft materials combining these properties together, fabrication of an engineering device, is still a challenge among the devices. Strain sensors bear the function to detect mechanical deformations due to elongation, flexure, or expansion.[1–5] Currently, a variety of stretchable strain sensors based on different mechanisms, including resistance,[6,7] capacitance,[8–10] fiber Bragg grating,[11] triboelectricity,[12] piezoelectricity,[13] and so forth,[14,15] have been explored. Particularly, a resistance-type sensor has superiority in furnishing with simple device structures, relatively easy readout systems, and high stretchability.[16] Abundant conductive materials, including carbon materials (e.g., carbon nanotube, graphene), metal materials (e.g., Ag nanowire, liquid metal), and conductive polymers (e.g., polyaniline), have been used to fabricate resistance-type strain sensors.[17] While conventional structures show minimum strain under operations, soft robotics and wearable electronics require orders of magnitude higher strain in operations. Devices or strain sensors to provide such a large measure are scarce. More interestingly, enabling these devices with self-healing soft materials can equip them with recovery and functional restoration after even severe damage, potentially prolonging the service life of these devices.[18–22] Some self-healing strain sensors based on rubber,[23] polyurethane composite,[24] and polyborosiloxane[25] have been fabricated by introducing reversible bonds (e.g., hydrogen bond, disulfide bond, and dative bonds) to endow self-healing capacity to the materials. However, none of these self-healing strain sensors can be stretched over 300%. Moreover, under high-strain operation, it is expected that a sensor can maintain its contact with moving/stretched object and, at same time, provide electric signals. Overall, a new material with high stretchability, strong adhesion, excellent self-healing after damage, and sensitivity to resistance is highly favored. Once successful, this material can be exploited to develop soft sensors for rehabilitation/personal health monitoring, sensory skin, sports performance monitoring, and motion capture in human body. Unfortunately, the largest strain in most reported self-healing and conductive materials is low.[23,26,27] Moreover, when a large strain is applied, the sensors assembled with materials show low sensitivity or low gauge factor

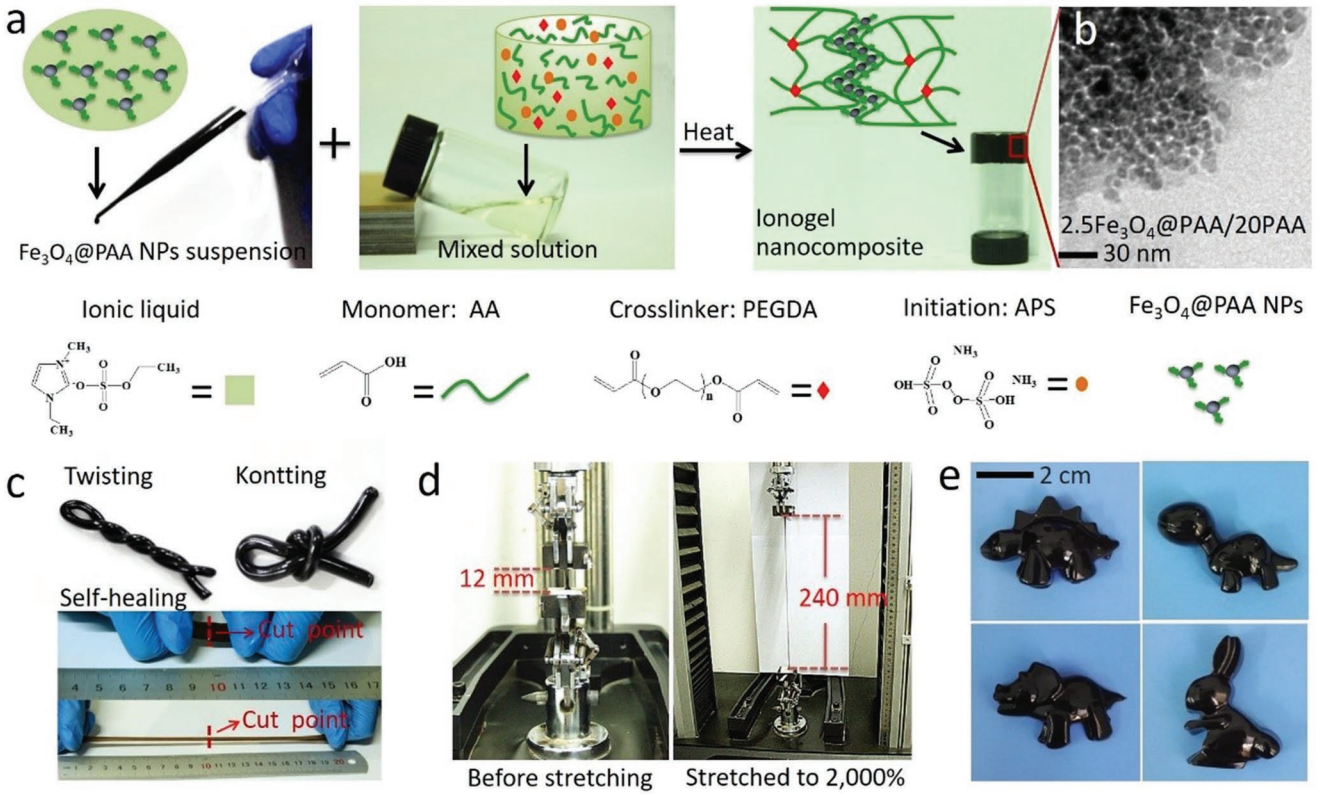

Figure 1. Design and fabrication of multifunctional Fe_3O_4@PAA/PAA ionogel nanocomposites. a) Schematic illustration of preparation procedures of the ionogel nanocomposites and chemical structures of the reagents. b) TEM image of the nanoparticles well dispersed within the $2.5Fe_3O_4$@PAA/20PAA sample. c) The $1.5Fe_3O_4$@PAA/20PAA sample was strong and tough enough to undergo twisting and knotting, and the self-healed sample could sustain ten times stretching. d) The $0.5Fe_3O_4$@PAA/20PAA sample could be stretched to 2000%. e) The sample could be made into different complex shapes of dinosaurs, cow, and rabbit.

(GF, defined as $\delta(\Delta R/R_0)/\delta\varepsilon$, where R_0 is the resistance of the unloaded sample, ΔR is the change of resistance, and ε is the applied strain). For example, a self-healable hydrogel with a large strain (≈1000%) only has a GF of 1.51.[28] Besides, water evaporation from the hydrogel significantly degrades the device performance with time.[29] It is still a challenge to develop a soft nonvolatile material with the combined features of self-healing, adhesion, and high stretchability for fabricating strain sensors that can detect extremely large deformation.

Herein, we developed a novel type of ionogel nanocomposite that is self-healing, adhesive, and highly stretchable for strain sensors. This material can be tuned by modifying the composition to achieve its best performances, including excellent stretchability (2000% tensile strain), conductivity (10^{-1} S m^{-1}), strong adhesion (347.3 ± 6.97 N m^{-1}), and remarkable self-healing capability upon cutting-induced failure. These performances are evidenced by a fast (0.5 s) and complete recovery (≈100%) in conductance, high tensile stress (96.5 ± 0.5%), and strain (98.7 ± 0.7%) after autonomous self-healing. We show here for the first time that a multifunctional strain sensor with a high GF and reliability under large deformation can be fabricated by ionogel nanocomposite. We believe that this opens up a new horizon for developing a self-healing and extremely large strain sensor that can be conformably integrated with arbitrary curved and moving surface.

The key to our success is the integration of metal coordination bonds in a loosely cross-linked network of ionogel. In order to achieve a homogeneous integration, we chose Fe_3O_4 nanoparticles (NPs) that were coated with poly(acrylic acid) (PAA) polymer (dubbed as Fe_3O_4@PAA NPs) (Figure S1, Supporting Information).[30] The gelation process started by mixing monomer (acrylic acid), cross-linker (poly(ethylene glycol) diacrylate), thermal initiator (ammonium persulfate), and Fe_3O_4@PAA NPs into ionic liquid ([C_2mim][$EtSO_4$], $C_8H_{16}N_2O_4S$). Then, the mixture was transformed to ionogel via a one-pot method at 60 °C (**Figure 1**a). Figure S2a (Supporting Information) shows the X-ray diffraction pattern of the Fe_3O_4@PAA NPs embedded in ionogel matrix, indicating that the Fe_3O_4 nanoparticles in the composite were pure Fe_3O_4 with inverse spinel structure. Transmission electron microscopy (TEM) image demonstrated that the Fe_3O_4@PAA NPs were well dispersed within the ionogel matrix (Figure 1b). According to the content of NPs (x) and PAA (y) relative to the total weight of the nanocomposite, we assign $x$$Fe_3O_4$@PAA/$y$PAA for each batch of the ionogel nanocomposites. For example, the $2.5Fe_3O_4$@PAA/20PAA sample contains 2.5 wt% NPs and 20 wt% PAA. We expect the addition of low percentage of cross-linker (0.3 wt%) to produce a loosely cross-linked network of PAA to fabricate soft gels for large strain sensors. Meanwhile, metal coordination bonds (Fe(III)—$O_{carboxyl}$) derived from exposed Fe(III) ions on Fe_3O_4 NP surface will be established within a

rich PAA matrix (Raman spectroscopy analysis; Figure S2b, Supporting Information).[31,32] The reversible nature of dynamic bonds including Fe(III)—$O_{carboxyl}$ coordination bonds (interaction of exposed Fe(III) ions on Fe_3O_4 NPs surface with rich carboxyl groups dangling on PAA chains), hydrogen bonds (interaction of carboxyl groups), and the ionic bonds (interaction of anionic carboxyl groups and cationic imidazolium ring) serves as sacrificial bonds to endow self-healing capability to the nanocomposite. Moreover, the reversible bonds around cracking zones will form more "new bridges" quickly between the two interfaces to enhance the interaction ability of polymer chains and nanoparticles for self-healing. Thus, a strip sample could autonomously self-heal to its initial shape after being cut by a scalpel. The healed strip could be stretched more than ten times of its original length without any observable damage. Moreover, this ionogel nanocomposite shows high level flexibility in knotting, twisting, and stretching (Figure 1c,d), as well as could be freely modeled to different complex shapes, such as dinosaurs and rabbit (Figure 1e). The ionogel nanocomposite cannot freely stand in the absence of chemical cross-linker. In the absence of the chemical cross-linker, the PAA polymer chains easily wrap around the Fe_3O_4@PAA NPs, giving rise to a viscous mixture rather than a rigid solid (Figure S3, Supporting Information). On the other hand, the absence of Fe_3O_4@PAA NPs delivers a PAA ionogel with poor self-healing capability (Figure S5, Supporting Information).

The ionogel nanocomposites are tough, stretchable, and self-healable. A sheet of 2.5Fe_3O_4@PAA/20PAA (30.0 × 30.0 × 1.0 mm^3) covered on an air pipe (inner diameter: 4 mm) can be inflated to a large balloon, and the strain area of the balloon was about 1100% at 3 s calculated from Figure S4 and Movie S1 (Supporting Information). Low Young's modulus (6.7–35.8 kPa) (Figure S6, Supporting Information) attributes large deformation to the nanocomposites. Then we cut the cross in the center of another 2.5Fe_3O_4@PAA/20PAA sample and subsequently put four pieces of the cut sample together to allow autonomous self-healing at room temperature (**Figure 2**a). Optical microscope images showed that the boundary of scar on the damaged sample almost disappeared after healing for 4 h without any assistance external energy (Figure 2b). While the self-healed sample expanded with inflation until strain up to 1300%, no leakage was observed (Figure 2a; Movie S1, Supporting Information).

The weight contents of PAA and Fe_3O_4@PAA NPs have effect on the self-healing property of the ionogel nanocomposites. The healing efficiency is defined as the ratio of the stress or strain of the healed (S_h) and pristine samples (S_p), i.e., HE = S_h/S_p. The healing efficiency of ionogel nanocomposites increases with the increase of PAA and NP contents (Figure S5, Supporting Information). A high healing efficiency of the 2.5Fe_3O_4@PAA/20PAA sample increases to 96.5 ± 0.5% of tensile stress and 98.7 ± 0.7% of ruptured strain when the samples self-healed at room temperature for 12 h. The mechanism of self-healing ability can be mainly attributed to the dynamic and reversible bonding feature of the Fe(III)—$O_{carboxyl}$ bond, allowing polymer network reorganization at the interface of fractured parts (Figure 2e), because the sample with high PAA content could provide more carboxyl groups to combine with Fe(III) at the fractured interface, thus promoting self-healing efficiency of the nanocomposite. The same mechanism is reasonable for the sample containing high NPs content. However, if excessive Fe_3O_4 content (more than 2.5 wt%) was added in the system, the nanocomposite cannot self-stand, because Fe(III) ions are quenchers of free radical polymerization,[33,34] hindering gelation of the nanocomposite (Figure S7, Supporting Information). Additionally, extra-high PAA content in the system (more than 40 wt%) leads to inhomogeneous ionogel nanocomposite.

Healing time also has effect on self-healing efficiency of the nanocomposite. Healing for long time leads to high recovered tensile stress and ruptured strain (Figure 2c). 90.9 ± 3.0% tensile stress and 92.8 ± 4.3% ruptured strain could be achieved for the 2.5Fe_3O_4@PAA/20PAA sample, after healing for 4 h at room temperature (see the bar graph in Figure 2c). The healed sample could be stretched to 1400% strain while keeping 37.3 kPa stress. In the process of stretching, the PAA polymer chains were elongated accompanying rupture of the dynamic Fe(III)—$O_{carboxyl}$ coordination bonding sites, and then after releasing the strain, Fe(III) ions could chelate with carboxyl groups again to reform new Fe(III)—$O_{carboxyl}$, initiating self-healing event of the ionogel nanocomposites (Figure 2e(i),(ii)). On the other hand, the loose chemical bonds between PAA polymer chains still connect, contributing to bearing strength.

In addition, healing temperature influences the self-healing efficiency of the nanocomposite. Our ionogel has low glass transition temperature (T_g, −51 °C) evidenced by a differential scanning calorimeter (Figure S8a, Supporting Information) and high thermal stability (250 °C) tested by thermogravimetric analysis (Figure S8b, Supporting Information), enabling the components in ionogel nanocomposites to freely rearrange and diffuse under low temperature, moreover, retaining stability at high temperature, contributing to self-healing behavior in a large temperature range. As expected, the Fe_3O_4@PAA/PAA displayed self-healing ability at −20 °C (Figure 2d). Temperature sweep of dynamic mechanical analysis demonstrated that the storage modulus of the 1.5Fe_3O_4@PAA/20PAA sample decreased from 2800.0 to 53.0 kPa when the sample was heated from −28 to 102 °C, indicating viscoelastic property of the ionogel nanocomposite and capability of equipment as strain sensors in large temperature range (Figure S9, Supporting Information). Increasing temperature can accelerate the free mobility of NPs and PAA polymer chains in the ionogel matrix, thus facilitating self-healing efficiency. The strain healing efficiency increased from 65.8 ± 0.9% to 88.8 ± 3.0% after healing for 2 h, when temperature increased from −20 to 60 °C. The wide healing temperature window satisfies the application of ionogel nanocomposite in harsh conditions.

The nanocomposite is also adhesive, which could achieve strong, rapid adhesion on substances at room temperature. For example, when a piece of 0.5Fe_3O_4@PAA/20PAA was slightly pressed onto the surface of copper or polydimethylsiloxane (PDMS) substrate, a strong automatic adhesion was observed after a few seconds of contact, and the lap junction could hold the weight of adhered substances, not requiring any glue or extra energy (Movie S2, Supporting Information). We quantitatively characterized the adhesion strength, i.e., failure force per unit width of the sample, by a lap-shear test

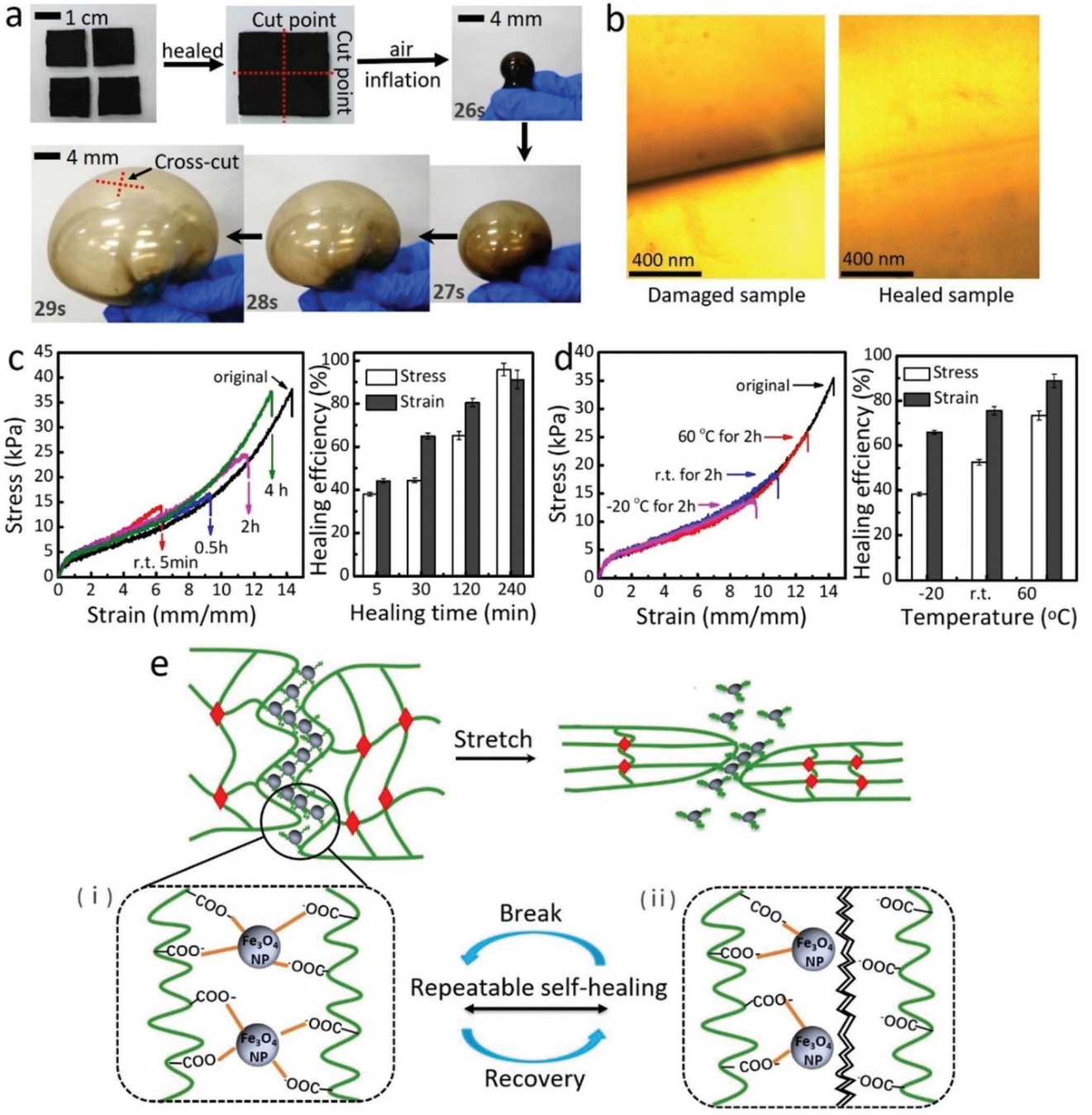

Figure 2. Self-healing and mechanical properties of the ionogel nanocomposites. a) Air inflation experiment of a self-healed ionogel nanocomposite balloon. A piece of square sample was cut into four pieces from middle; after healing for 4 h, the healed sample could be inflated into a balloon. b) Optical microscope images of the damaged and self-healed samples. The effect of c) healing time and d) healing temperature on the tensile stress and healing efficiency of the nanocomposites. e) Schematic illustration of stretched PAA networks of the ionogel nanocomposites, and self-healing mechanism of dynamic association and dissociation of the reversible coordination bonds of Fe(III)$-O_{carboxyl}$ (i, ii). All the tests used the 2.5Fe_3O_4@PAA/20PAA ionogel nanocomposite.

(photograph inset in **Figure 3**a,b). The adhesion strength of copper sheet is 347.3 ± 6.97 N m^{-1}, which is obviously large than that of PDMS (207.4 ± 24.98 N m^{-1}) (Figure 3c), demonstrating that the adhesion of nanocomposite to metallic element is higher than that of polymer elastomer. It is reasonable that the metal coordination between carboxyl groups of PAA polymer chains and metallic element is stronger than that between the nanocomposite and PDMS due to lack of specific interaction. The excellent adhesion achieved here is benefit for the nanocomposite to adhere and connect with metal electrode or polymer substrate used in the electronic system.

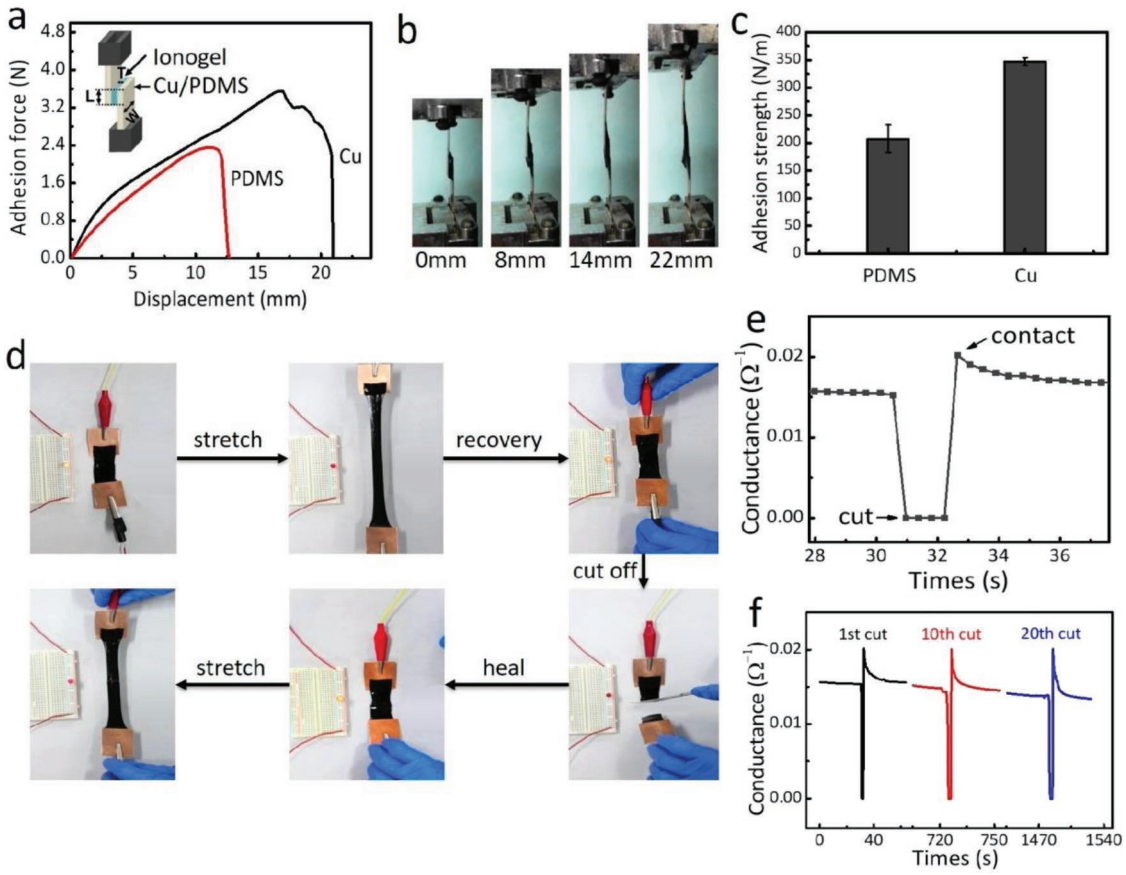

Figure 3. Self-adhesion and electrical performance of the ionogel nanocomposite. a) Adhesion force–displacement curves of sample to copper and PDMS (inset photograph is the lap-shear adhesive testing geometry). b) Photographs of lap-shear tests of two copper sheets adhered with ionogel. The sample could be highly stretched before peeling off from copper sheets. c) Adhesion strength of ionogel adhered on PDMS and copper. d) The ionogel as a conductor assembled in a circuit with a red LED bulb. The LED flickered on complete release of tensile strain, and the LED immediately flickered when the sample self-healed after cut. e) Time dependence of conductance and healing speed of the sample. f) Repeated electrical healing of 10 and 20 times cuts at same severed location. All the tests used the 1.5Fe_3O_4@PAA/20PAA ionogel nanocomposite.

A 2.5Fe_3O_4@PAA/20PAA strip can be settled into circuit and directly connected with two sheets of copper electrodes without any glue (Figure 3d). The adhesion between the nanocomposite and electrodes is enough to endure the force in the course of circuit stretching, and accompanying with ≈4 times stretching of the nanocomposite. The light-emitting diode (LED) in the circuit obviously became less bright with an increase of strain deformation, showing its sensing capability in the deformation process. Moreover, the LED immediately reproducibly flickered in 21 s (Movie S3, Supporting Information) when the nanocomposite healed after breaking. Even cutting the sample at the same place for 20 times, the conductance of the self-healed sample could recover to its original value (≈ 0.015 Ω^{-1}) in 0.5 s (Figure 3e,f), demonstrating excellent repeatable restoration of electrical performance of the nanocomposites.

The nanocomposite can be used for assembling of strain sensors. We analyzed the variation of electrical signals with the change of external strain. The resistance of ionogel, $R = \rho L/S$ (where ρ is the specific resistivity, L is the length, and S is the cross-sectional area), ρ, and volume $L \times S$ of the ionogel nanocomposite sample are constant values, thus inducing decrease of S with L elongation, resulting in the increase of R. Real-time resistance can be monitored while stretching, and the relative change of resistance $\Delta R/R_0 = (R - R_0)/R_0$ (where R_0 is the initial resistance of the sample at room temperature and R is the real-time resistance of the stretched sample) will be calculated. Under tension, $\Delta R/R_0$ of the 2.5Fe_3O_4@PAA/20PAA ionogel nanocomposite–based strain sensor increased continuously up to about 155 when the applied strain reached 1400% (**Figure 4**a). The $\Delta R/R_0$–strain curves of the original and healed samples were almost coincident. The slope of the fitted $\Delta R/R_0$–strain curve reflects GF, i.e., the sensitivity of the sensor to strain. When the strain was less than 800%, the calculated GF values were 3.82 ± 0.1 and 3.96 ± 0.12 for original and healed samples, respectively, and the fitted Pearson's r values were 0.98858 and 0.98887, respectively, which indicates the superior piecewise linearity of its application as a sensor and is conducive to subsequent signal processing. When the applied strain was as high as 800–1400%, the GF values of original and healed samples increased to 19.6 ± 0.33 and 20.2 ± 0.54, respectively, and the fitted Pearson's r values were 0.99485 and 0.99462, respectively. Meanwhile, the sensor exhibited small hysteresis behavior under a constant strain rate of 100 mm min^{-1}, and the phenomenon is mainly attributed to the viscoelastic property

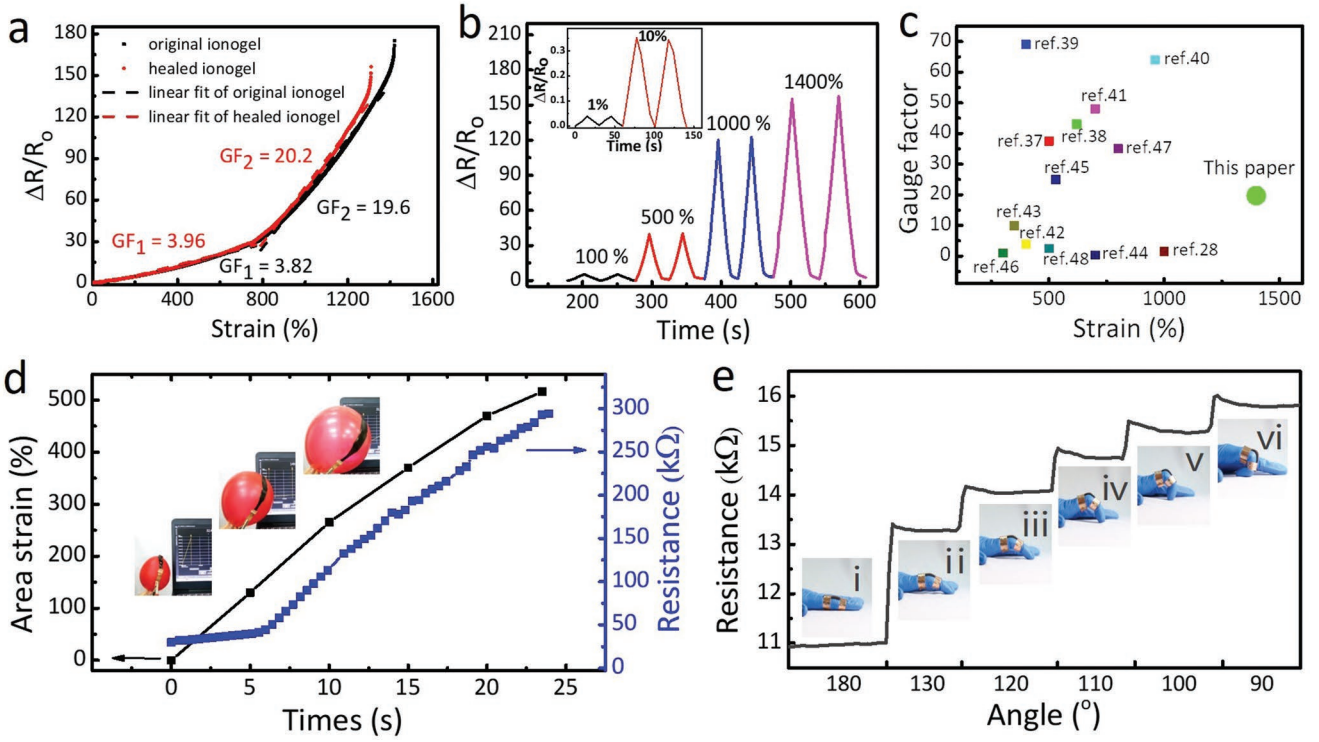

Figure 4. The ionogel nanocomposite–based conformal strain sensor. a) Relative change in resistance ($\Delta R/R_o$) versus strain of an original and a self-healed 2.5Fe_3O_4@PAA/20PAA sample. b) Reversible response of the ionogel nanocomposite–based strain sensor to the loading/unloading cycles of strain with various tensile strains from 1% to 1400%. c) Summary of relationship between gauge factor and strain of reported stretchable strain sensors (strain >300%). d) The dependence of area strain (left) and resistance (right) of a self-healed 2.5Fe_3O_4@PAA/20PAA-based strain sensor attached to an air inflating balloon. e) The 1.5Fe_3O_4@PAA/20PAA-based strain sensor fixed on forefinger of a human finger to monitor bending motions, via the change of corresponding resistance. Bending forefinger gradually changed to 90° from standard position, and the resistance of sensor also corresponded to increase.

of the ionogel nanocomposite[35,36] (Figure S11a, Supporting Information). The strain sensors also retained their sensing performance in the process of continuous deformation, under both large (1400%) and small (1%) loading/unloading cycles. Moreover, their electrical resistance almost completely recovered upon release of tensile strain in each cycle (Figure 4b). The ionogel nanocomposite–based strain sensor demonstrates high GF with the largest deformation compared with previously reported stretchable strain sensors (Figure 4c),[28,37–48] and its sensitivity is also much higher than many of the reported results such as strain sensors based on typical metal (≈2 at 5% strain),[38,49] ionic conductor (0.348 ± 0.11 at 700% strain),[44] and hydrogel (1.51 at 1000% strain).[28] The results demonstrate that our ionogel nanocomposite–based strain sensor is capable of measuring strain from 1% to 1400% with high stretching sensitivity, whether it was assembled by original or self-healed sample.

The reliability of the ionogel nanocomposite–based strain sensor was examined at 100 mm min^{-1} deformation rate. As shown in Figure S11b,c (Supporting Information) under 1400% strain loading and unloading cycles, before 100 cycles, there is a very slow growth in both wave crest and valley of $\Delta R/R_o$ value due to residual deformation of the nanocomposites. Until around 100 cycles, the wave crest of $\Delta R/R_o$ increased about 50 and the valley increased about 30, indicating that some creeps were generated in this long-time repeated loading.[50] However, the wave shape of the sensor remained unchanged after 100 cycles, implying good reliability and excellent durability of the ionogel nanocomposite–based strain sensors.

The multiple merits make the strain sensor based on our nanocomposite unique and interesting. For example, in the case of monitoring of balloon expansion, existing strain sensors hardly accommodate large dynamic deformation because of the lack of adhesion and stretchability. We loaded the healed 2.5Fe_3O_4@PAA/20PAA sample (healed for 4 h at room temperature) on the surface of balloon before inflation (Figure 4d). The healed strain sensor could conform and firmly attach to arbitrary surface of the balloon without peeling off, deforming with balloon expansion (Movie S4, Supporting Information). The resistance of sensor increased from 32.4 to 312 kΩ as area strain of the balloon increased 500% in 23 s. It is worth noting that the healed ionogel nanocomposite combined with two cut pieces can sustain large deformation and there was no splitting in the process of balloon expansion. This demonstrates that the nanocomposite-based strain sensors are able to conform and attach to arbitrary surface, sensitively monitoring the volume change, and even the self-healed sample still can be normally operated under large deformation.

The strain sensor could detect small deformation as well, such as motion of finger bending. A strip of nanocomposite was fixed to the forefinger of a human hand by two copper electrode rings. The resistance of the strain sensor sensitively

increased to different levels with an increase of step-by-step bending movements (Figure 4e). The proof-of-concept strain sensor with the advantages of self-healing, adhesion, stretchability, and high sensitivity holds great potential for exploring various large strain sensors.

In summary, we report a novel approach to prepare ionogel nanocomposite with unprecedented mutifunctions, including remarkable self-healing, strong adhesion, and high stretchability. The nanocomposite-based strain sensor can detect large deformation of arbitrary curved and moving object. Strategic dual cross-linking sites, i.e., reversible Fe(III)$-O_{carboxyl}$ metal coordination bonds and loosely covalent cross-links, were achieved for obtaining the multifunctional nanocomposite. A proof-of-concept ionogel-based strain sensor with high sensitivity was demonstrated by changing electrical resistance with special distortion, like arbitrary curved and moving surface of balloon inflation, as well as common deformation (e.g., large stretching and finger bending). We believe that the multifunctional nanocomposite-based strain sensor exhibits a great potential to detect large deformation objects with high sensitivity, such as stretching of airplane wings, wearable electronics and smart clothes, human/machine interfaces, soft robotics, and entertainment fields.

Experimental Section

Experimental details are given in the Supporting Information.

Supporting Information

Supporting Information is available from the Wiley Online Library or from the author.

Acknowledgements

This work was supported by the National Natural Science Foundation of China (no. 11674263), International Science & Technology Cooperation Program supported by Ministry of Science and Technology of China and Shaanxi Province (2013KW14-02), the Program for the Key Science and Technology Innovative Team of Shaanxi Province (no. 2013KCT-05), Collaborative Innovation Center of Suzhou Nano Science and Technology, and Suzhou Research Institute.

Conflict of Interest

The authors declare no conflict of interest.

Keywords

adhesion, ionogel nanocomposites, self-healing, strain sensors, stretchability

Received: November 7, 2018
Revised: March 17, 2019
Published online:

[1] G. Shi, Z. Zhao, J.-H. Pai, I. Lee, L. Zhang, C. Stevenson, K. Ishara, R. Zhang, H. Zhu, J. Ma, *Adv. Funct. Mater.* **2016**, *26*, 7614.
[2] J. Y. Sun, C. Keplinger, G. M. Whitesides, Z. Suo, *Adv. Mater.* **2014**, *26*, 7608.
[3] I. You, B. Kim, J. Park, K. Koh, S. Shin, S. Jung, U. Jeong, *Adv. Mater.* **2016**, *28*, 6359.
[4] Y. Heo, Y. Hwang, H. S. Jung, S. H. Choa, H. C. Ko, *Small* **2017**, *13*, 1700070.
[5] Y. Li, Y. A. Samad, T. Taha, G. Cai, S.-Y. Fu, K. Liao, *ACS Sustainable Chem. Eng.* **2016**, *4*, 4288.
[6] S. Chen, Y. Song, D. Ding, Z. Ling, F. Xu, *Adv. Funct. Mater.* **2018**, *28*, 1802547.
[7] D. Y. Choi, M. H. Kim, Y. S. Oh, S. H. Jung, J. H. Jung, H. J. Sung, H. W. Lee, H. M. Lee, *ACS Appl. Mater. Interfaces* **2017**, *9*, 1770.
[8] A. Atalay, V. Sanchez, O. Atalay, D. M. Vogt, F. Haufe, R. J. Wood, C. J. Walsh, *Adv. Mater. Technol.* **2017**, *2*, 1700136.
[9] O. Atalay, *Materials* **2018**, *11*, 768.
[10] A. Fassler, C. Majidi, *Smart Mater. Struct.* **2013**, *22*, 055023.
[11] C. E. Campanella, A. Cuccovillo, C. Campanella, A. Yurt, V. M. N. Passaro, *Sensors* **2018**, *18*, 3115.
[12] H. J. Sim, C. Choi, S. H. Kim, K. M. Kim, C. J. Lee, Y. T. Kim, X. Lepro, R. H. Baughman, S. J. Kim, *Sci. Rep.* **2016**, *6*, 35153.
[13] W. Wu, L. Wang, Y. Li, F. Zhang, L. Lin, S. Niu, D. Chenet, X. Zhang, Y. Hao, T. F. Heinz, J. Hone, Z. L. Wang, *Nature* **2014**, *514*, 470.
[14] C. Wang, D. Hwang, Z. Yu, K. Takei, J. Park, T. Chen, B. Ma, A. Javey, *Nat. Mater.* **2013**, *12*, 899.
[15] Y. Zang, F. Zhang, D. Huang, X. Gao, C. A. Di, D. Zhu, *Nat. Commun.* **2015**, *6*, 6269.
[16] X. Liao, Z. Zhang, Q. Liang, Q. Liao, Y. Zhang, *ACS Appl. Mater. Interfaces* **2017**, *9*, 4151.
[17] T. Q. Trung, N. E. Lee, *Adv. Mater.* **2017**, *29*, 1603167.
[18] P. J. M. Monteiro, S. A. Miller, A. Horvath, *Nat. Mater.* **2017**, *16*, 698.
[19] T. L. Sun, T. Kurokawa, S. Kuroda, A. B. Ihsan, T. Akasaki, K. Sato, M. A. Haque, T. Nakajima, J. P. Gong, *Nat. Mater.* **2013**, *12*, 932.
[20] S. Gupta, Q. Zhang, T. Emrick, A. C. Balazs, T. P. Russell, *Nat. Mater.* **2006**, *5*, 229.
[21] H. Wang, B. Zhu, W. Jiang, Y. Yang, W. R. Leow, H. Wang, X. Chen, *Adv. Mater.* **2014**, *26*, 3638.
[22] J. Kang, D. Son, G.-J. N. Wang, Y. Liu, J. Lopez, Y. Kim, J. Y. Oh, T. Katsumata, J. Mun, Y. Lee, L. Jin, J. B.-H. Tok, Z. Bao, *Adv. Mater.* **2018**, *30*, 1706846.
[23] X. Liu, C. Lu, X. Wu, X. Zhang, *J. Mater. Chem. A* **2017**, *5*, 9824.
[24] T. P. Huynh, P. Sonar, H. Haick, *Adv. Mater.* **2017**, *29*, 1604973.
[25] E. D'Elia, S. Barg, N. Ni, V. G. Rocha, E. Saiz, *Adv. Mater.* **2015**, *27*, 4788.
[26] T. P. Huynh, H. Haick, *Adv. Mater.* **2016**, *28*, 138.
[27] Y. Shi, M. Wang, C. Ma, Y. Wang, X. Li, G. Yu, *Nano Lett.* **2015**, *15*, 6276.
[28] G. Cai, J. Wang, K. Qian, J. Chen, S. Li, P. S. Lee, *Adv. Sci.* **2017**, *4*, 1600190.
[29] H. Yuk, T. Zhang, G. A. Parada, X. Liu, X. Zhao, *Nat. Commun.* **2016**, *7*, 12028.
[30] H. Haider, C. H. Yang, W. J. Zheng, J. H. Yang, M. X. Wang, S. Yang, M. Zrínyi, Y. Osada, Z. Suo, Q. Zhang, J. Zhou, Y. M. Chen, *Soft Matter* **2015**, *11*, 8253.
[31] Q. Li, D. G. Barrett, P. B. Messersmith, N. Holten-Andersen, *ACS Nano* **2016**, *10*, 1317.
[32] Z. Wei, J. He, T. Liang, H. Oh, J. Athas, Z. Tong, C. Wang, Z. Nie, *Polym. Chem.* **2013**, *4*, 4601.
[33] C. H. Bamford, A. D. Jenkins, R. Johnston, *Proc. R. Soc. London, Ser. A* **1957**, *239*, 214.
[34] E. Collinson, F. S. Dainton, *Nature* **1956**, *177*, 1224.
[35] M. Amjadi, M. Turan, C. P. Clementson, M. Sitti, *ACS Appl. Mater. Interfaces* **2016**, *8*, 5618.

[36] Y. Lin, X. Dong, S. Liu, S. Chen, Y. Wei, L. Liu, *ACS Appl. Mater. Interfaces* **2016**, *8*, 24143.
[37] C. Wang, X. Li, E. Gao, M. Jian, K. Xia, Q. Wang, Z. Xu, T. Ren, Y. Zhang, *Adv. Mater.* **2016**, *28*, 6640.
[38] S. Tadakaluru, W. Thongsuwan, P. Singjai, *Sensors* **2014**, *14*, 868.
[39] P. Slobodian, P. Riha, R. Benlikaya, P. Svoboda, D. Petras, *IEEE Sens. J.* **2013**, *13*, 4045.
[40] S. Ryu, P. Lee, J. B. Chou, R. Xu, R. Zhao, A. J. Hart, S.-G. Kim, *ACS Nano* **2015**, *9*, 5929.
[41] S.-J. Park, J. Kim, M. Chu, M. Khine, *Adv. Mater. Technol.* **2016**, *1*, 1600053.
[42] J. T. Muth, D. M. Vogt, R. L. Truby, Y. Menguc, D. B. Kolesky, R. J. Wood, J. A. Lewis, *Adv. Mater.* **2014**, *26*, 6307.
[43] S. Gong, D. T. H. Lai, B. Su, K. J. Si, Z. Ma, L. W. Yap, P. Guo, W. Cheng, *Adv. Electron. Mater.* **2015**, *1*, 1400063.
[44] A. Frutiger, J. T. Muth, D. M. Vogt, Y. Menguc, A. Campo, A. D. Valentine, C. J. Walsh, J. A. Lewis, *Adv. Mater.* **2015**, *27*, 2440.
[45] M. A. Darabi, A. Khosrozadeh, Q. Wang, M. Xing, *ACS Appl. Mater. Interfaces* **2015**, *7*, 26195.
[46] L. Cai, L. Song, P. Luan, Q. Zhang, N. Zhang, Q. Gao, D. Zhao, X. Zhang, M. Tu, F. Yang, W. Zhou, Q. Fan, J. Luo, W. Zhou, P. M. Ajayan, S. Xie, *Sci. Rep.* **2013**, *3*, 3048.
[47] C. S. Boland, U. Khan, C. Backes, A. O'Neill, J. McCauley, S. Duane, R. Shanker, Y. Liu, I. Jurewicz, A. B. Dalton, J. N. Coleman, *ACS Nano* **2014**, *8*, 8819.
[48] M. Amjadi, Y. J. Yoon, I. Park, *Nanotechnology* **2015**, *26*, 375501.
[49] M. Amjadi, A. Pichitpajongkit, S. Lee, S. Ryu, I. Park, *ACS Nano* **2014**, *8*, 5154.
[50] M. Leocmach, C. Perge, T. Divoux, S. Manneville, *Phys. Rev. Lett.* **2014**, *113*, 038303.